J Mater Sci (2006) 41:7165–7182
DOI 10.1007/s10853-006-0923-9

Effect of contact geometry on compressive failure processes in sandwich structures

Witolda A. Maruszewska · John P. Dear

Received: 31 October 2005 / Accepted: 7 December 2005 / Published online: 4 October 2006

Abstract Reducing the unladen weight of road and rail vehicles as well as ships and aircraft is often a requirement. This is to increase their performance, achieve better fuel economy, reduce direct operating costs and make other improvements as new suitable lightweight materials become available. However, at the design stage, often it is also needed to assess the lightweight or other candidate materials as to their ability to absorb impact energy in the event of a crash or other major impact. Related to the use of lightweight materials in racing car bodies, the Federation International de L'Automobile (FIA) has introduced stringent methods for assessing lightweight and other structural materials particularly as to their ability to protect racing car drivers in the advent of a crash. However, this FIA assessment method requires large sheets of material and a very powerful impact facility. One aim of this study was to devise a scaled down method that was able to provide data relatable to those from the full-scale FIA evaluation. This is together with providing for varying the impact conditions to study the variability of material properties in panels. Also, this is to explore the properties of lightweight materials for other applications as to their high-energy absorption ability.

W. A. Maruszewska · J. P. Dear (✉)
Department of Mechanical Engineering, Imperial College London, South Kensington, Exhibition Road, London SW7 2AZ, UK
e-mail: j.dear@imperial.ac.uk

Introduction

The FIA impact assessment [1] is part of the ultimate and final accreditation of material for F1 racing cars and uses large material specimens and powerful impact facilities [2]. However, when developing new materials, investigating crash damaged material and making preliminary studies of candidate materials, it is the ability to research the impact properties using small samples of material that is often needed. Also, the smaller the specimen the more it is possible to explore more fully the variability of properties in produced material. In this research, the interest was to study in detail the physical characteristics of different lightweight composite sandwich materials. This is as to their loss of stiffness during impact, the impact energy absorbed by the damage processes and the retention of integrity of the material at different stages of the impact. The aim was to achieve small-scale impact data comparable to those generated by the large-scale FIA assessment method. The devised smaller scale assessment method uses a truncated cone impactor similar to that employed by the FIA but of a reduced size. In addition, for the small-scale studies, a hemispherical impactor is also used. The latter was to gain more information about the impact failure processes in the core material. Important was that the smaller impactors needed to be of a size to crush a substantial volume of the sandwich core material [3].

A great deal of research has been devoted to sheet composite materials [4–10] but less so for honeycomb sandwich materials for the type of impact conditions researched in this study. Harrigan, Reid and Peng [11] have studied crush processes in aluminium honeycomb showing the good energy absorbing properties of these

lightweight materials. Langdon, Cantwell and Nurick [12] have shown that combining glass fibre reinforced polypropylene composites and aluminium layers to produce fibre–metal laminates can give very high impact energy absorption ability. This ability to absorb impact energy is linked to the presence of many interfaces e.g. delamination in the composite, debonding between aluminium and composite as well as spalling and petalling of the aluminium. Such failure mechanisms are also observed in laminated glass and other composite structures [13, 14]. Herup and Palazotto [15] have studied the low velocity impact performance of laminates with a composite skin and Nomex honeycomb and found the c-scan technique useful in observing development of damage. Abrate [16], Mines, Worrall and Gibson [17], and Olsson [18] have independently compared for sandwich panels of both aluminium and Nomex honeycomb the impact conditions for upper skin failure, core crush, lower skin failure and perforation and have linked the different stages of failure to the force-time traces.

Anderson and Madenci [19] have characterised the type and extent of damage observed in a variety of sandwich configurations with graphite/epoxy skins and foam or honeycomb cores. Residual indentation observed using cross-sectional views of the impacted specimens provided a good criterion of damage. It was found that although the skin surfaces can exhibit very little damage at low impact energies, there can be significant levels of internal damage to the core. Akil Hazizan and Cantwell [20] examined the low velocity impact response of two aluminium honeycomb sandwich structures with glass fibre reinforced epoxy skins. The impact response was modelled with an energy-balance model, which accounted for energy absorption in bending, shear and contact effects. This gave good agreement and it was shown that the partitioning of the incident energy depended upon the geometry of the impacting projectile. Roach, Evans and Jones [21] have studied in detail glass–fibre polyester skins with and without a structural PVC foam foundation. It was shown that there is a good correlation between impact energy and the area of damage for impact velocities up to 120 m/s particularly for the foam-backed laminates. Shyr and Pan [22] investigated an integrated hollow pile glass fabric and non-woven mat, inlaid into a multiaxial warp knit blanket, which was laminated to form a sandwich structure and a hybrid structure. The results showed that the inlaid materials played an important role in the impact behaviour and damage characteristics of the laminates.

The first objective in this study was to devise a special to purpose small impact test fixture that could be employed on a universal test machine, as available in most experimental laboratories, for the following research:

- To be able to explore the contact conditions as the impactor closed with the skin of the sandwich honeycomb material for both a truncated cone and a hemispherical impactor.
- To determine, during the loading event, the period for the different sandwich materials that the skin was able to spread the impact force before starting to fail and the following skin failure process.
- To observe the crushing of the core as to the extent it spread or remained confined to the zone immediately under the nose of the truncated cone and hemispherical impactors.
- To study the extent of core damage before and after the failure of the rear skin related to the energy absorption of the material during the impact event.

These data were needed to relate energy absorbing ability of the different sandwich materials studied to their loss of stiffness, strength and integrity at different stages of the loading sequences.

Experimental

Development of the experimental facility

A requirement is that the small-scale facility [23] needs to provide data relatable to those obtained from the FIA large-scale assessment facilities. However, it was also needed to provide impact energy absorption data useful in the development of lightweight materials for other applications. Design requirements for the small-scale test facility are as follows:

- To evaluate square specimens of sandwich material 150×150 mm.
- To be able to evaluate specimens up to 30 mm thick (5–30 mm). The facility needed to be designed to withstand a compressive load of 100 kN and this is without it distorting or losing its shape in any other way during the loading sequences.
- To provide for a sufficient number of honeycomb cells or other sandwich core features to be crushed and compacted so as to be able to assess fully the material's inherent impact energy absorption ability.
- To ensure that the specimens are appropriately constrained in a fixture so that the impact response of the specimen relates to the inherent properties of the panel material.

- To provide for the small-scale facility to use a truncated cone impactor and also other types of impact head so that a variety of comparisons can be made.

To satisfy the above requirements, the specimen's support frame for the small-scale experimental fixture was provided with a substantial stainless steel base. The specimen's retaining collars were also made of the same stainless steel. For this study, the experimental fixture was configured for use on an INSTRON 1186 test machine with a 200 kN rated load cell and the Instron had a very rigid specimen platform. This is important when determining the initial stiffness of the specimens from the load-displacement traces. The effective stiffness of the specimen support and crosshead are well in excess of the specimen stiffness. Also, extra care was needed to maintain correct alignment of the impact head to the centre of the specimen and to make sure the specimen could not make any unwanted movements during the loading sequence. Figure 1 shows a schematic of the experimental arrangement with Fig. 1a showing a plan view of the specimen and its retaining fixtures. Figure 1b shows a side-view of the specimen and the truncated-cone impactor in the INSTRON test machine.

Materials evaluated

For the development of the small-scale facility, three types of HEXCEL sandwich panels were selected for their different stiffness and energy absorption ability. For example, these are the types of structure currently used for lightweight components of racing car bodies and transport vehicles. These sandwich panels had different skin and core combinations. Table 1 are the data provided by the material manufacturer. For each material type, several samples were cut from a large single sheet of composite material. This was to provide for assessing the consistency of lay-up and other manufacturing process as to the effect on stiffness and energy absorption of the material.

Experimental methods

The compressive quasi-static experiments are performed, as described below, with the same set boundary conditions for all specimens. A fully instrumented INSTRON 1186 machine was used with a 200 kN load capacity and was controlled by a PC using INSTRON IX software. For each material, two types of impact head were used namely the small-scale truncated cone and the hemispherical impact head (see Fig. 1). These impact heads were attached to the load cell and fitted to the INSTRON fixed crossbeam. The specimens were secured to the lower moveable INSTRON crossbeam. From the start position, with the impact head just in contact with the specimen, the lower crosshead was raised at the required rate to compress the specimen and to drive the impact head into the sample for the required travel distance. For the experiments, a clear Perspex screen was used to retain the shards of composite breaking free of the deforming specimen. At the end of the programmed test, the compressive load with respect to displacement was logged by the data acquisition system. Data sampling was set at a rate of 18 points per second as this provided for obtaining good load versus displacement data with low noise in the traces.

The experimental conditions for the small-scale arrangement are as follows:

- Crosshead speed = 100 mm/min constant rate
- Total impactor travel = 50 mm
- Impactor datum = level with top skin
- Impactor shape = truncated cone (frustrum) with frontal diameter of 33 mm increasing to rear face diameter of 74 mm over a length of 82 mm *or* Impactor shape = hemisphere of diameter 74 mm.
- Samples restrained along the edges in all degrees of freedom
- Sample size = 150 × 150 mm square

Results

Truncated cone impactor

Figure 2 shows for each material the load versus displacement data for the truncated cone impact head. This is for four samples of H220 (Fig. 2a), four samples of H620 (Fig. 2b) and four samples of Fibrelam Grade 5 (Fig. 2c). Figure 3 shows a single load-displacement trace for each of the three types of sandwich panel (Fig. 3a) together with corresponding energy-displacement traces (Fig. 3b).

Figures 4–6 show the damage inflicted on the different types of sandwich panel for top, bottom and cross-sectional views. The damage inflicted on each of the four specimens for each type of sandwich panel was very similar. Figures 7–9 provide an illustration of the extent of damage inflicted on each type of sandwich panel at different stages of the impact related to the different phases of the load versus displacement traces.

In the case of H220, with aluminium skins and an aluminium honeycomb core, there are two main peaks

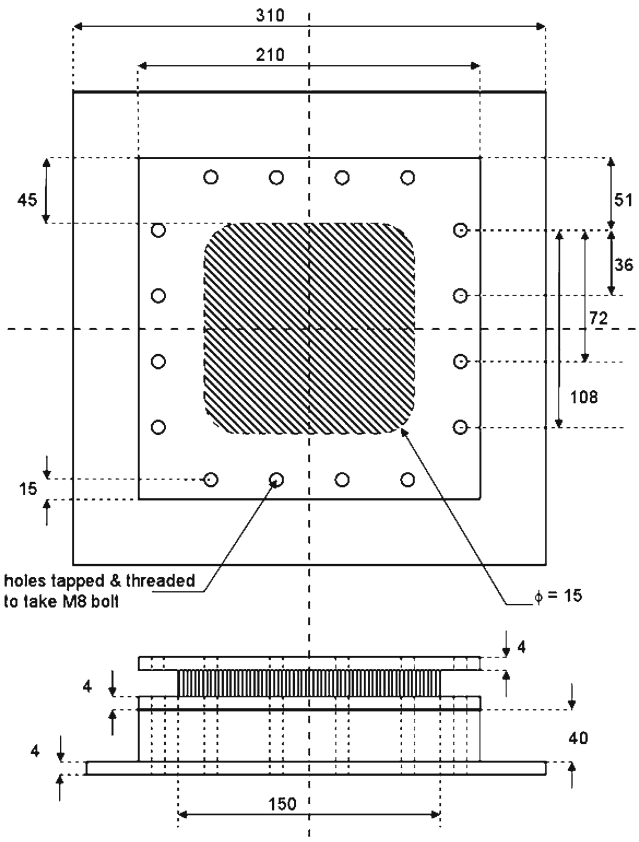

(a) Plan and edge view of specimen in retaining fixtures

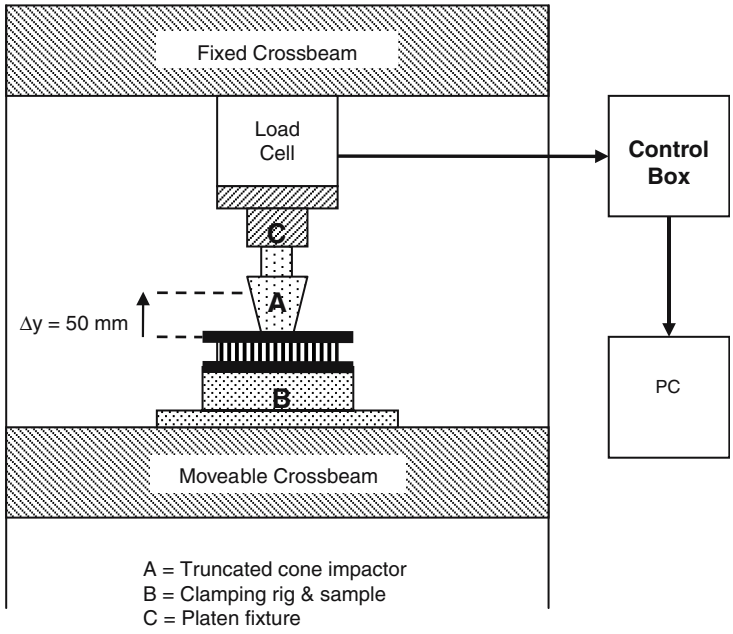

(b) Side view of the specimen in the Instron testing machine

Fig. 1 Schematic showing experimental arrangement: (**a**) plan and edge view of the specimen and its retaining fixtures with dimensions in mm; (**b**) side-view of the specimen in the INSTRON testing machine

on the load-displacement traces for the truncated cone impactor (see Fig. 2a). The first peak mostly relates to penetration of the front skin and between the first and second peak, damage relates mostly to the crushing of the core and the following penetration of the rear skin. Of the three panel types tested, only the H220 material

Table 1 Sample skin and core constituent materials and physical properties

Material	Construction of the sandwich materials	Weight (kg m^{-2})	Overall thickness (mm)	Skin thickness (mm)	Core density (kg m^{-3})	Cell size of core across flats (mm)
Hexlite (H 220)	Aluminium alloy sheet bonded to lightweight aluminium honeycomb using epoxy film adhesive	4.7	13.9	0.5	83	6.4
Hexlite (H 620)	Plain woven glass fibre impregnated with epoxy resin and a lightweight aluminium honeycomb core. (*Volume fraction of skin is 0.45*)	3.08	13.7	0.5 *1 ply per skin*	83	6.4
Fibrelam Grade 5	Unidirectional cross-plied fibreglass skins (S-glass) bonded to aramid (Kevlar/Phenolic) medium density core. (*Volume fraction of skin is 0. 5*)	2.5	10.16	0.38 *2 plies per skin*	80	3

exhibited complete perforation (see Fig. 4) of the structure for the truncated cone impactor.

For the H620 material with a woven composite skin and an aluminium honeycomb core, there are similarities with the H220 impact failure processes. However, notable for the truncated cone impactor, is that there is quite a lot of variability in the load versus displacement traces, for different specimens of the same material, after the front skin of the H620 specimens start to break up and the rear skin starts to become detached (see Fig. 2b). The H620 material sustained puncture of the top skin only for the truncated cone impactor (see Fig. 5) with the lower skin being detached from the core structure. This is as a result of the adhesive layer failure and in the process the lower skin is significantly deformed.

The Fibrelam Grade 5 material, with glass unidirectional cross-ply skins and an aramid core, exhibited a more gradual climb to the first peak of load with a higher sustained load plateau (see Fig. 2c). The Fibrelam Grade 5 does not exhibit the damage features exhibited in both Hexlite panels. In contrast, the primary damage relates to folding of the skins (see Fig. 6), particularly in areas where extensive core deformation is present. In combination with this core deformation, there is also a considerable amount of skin tear and this varies according to the orientation of the constituent fibres.

Hemisperical impactor

Figure 10 shows, for each material, the load versus displacement data for the hemispherical impact head. Again, this is for four samples of H220 (Fig. 10a), four samples of H620 (Fig. 10b) and four samples of Fibrelam Grade 5 (Fig. 10c). Figure 11 shows a single force-displacement trace for each of the three sandwich panel types (Fig. 11a) together with corresponding energy-displacement traces (Fig. 11b).

Figures 12–14 reveal the damage inflicted for a hemispherical impactor on the different types of specimen for top, bottom and cross-sectional views. Figures 15 –17 provide an illustration of the extent of damage inflicted on each type of sandwich panel at different stages of the impact related to the different phases of the load versus displacement traces.

For the H220 material, there is considerable difference in the load versus displacement traces for the hemispherical and truncated cone impactors. This is with the hemispherical impactor having two peaks of similar height and closer together than is the case for the truncated cone impactor. However, it is interesting to note that the total energy absorbed for H220, up to a displacement of 45 mm, is about 250 J for both impactors (see Figs. 3b and 11b) albeit there are notable differences in the type of damage inflicted by the hemispherical and the truncated cone impactor (see Figs. 4 and 12).

For the H620 material, the load versus displacement trace for the hemispherical impactor is quite smooth without peaks produced by the failures of the front and rear skins. However, there is a notable difference in the total energy absorbed for the truncated cone (350 J) and hemispherical (300 J) impact heads (see Figs. 3b and 11b). Mostly, this relates to the different damage inflicted on H620 specimens by the way the composite skins failed and broke away from the core material in the case of the truncated cone impact (see Figs. 5 and 13). For the hemispherical impactor on H620 in Fig. 13, there was no full penetration of the front skin and no major separation of the rear skin but significant general deformation of the specimen.

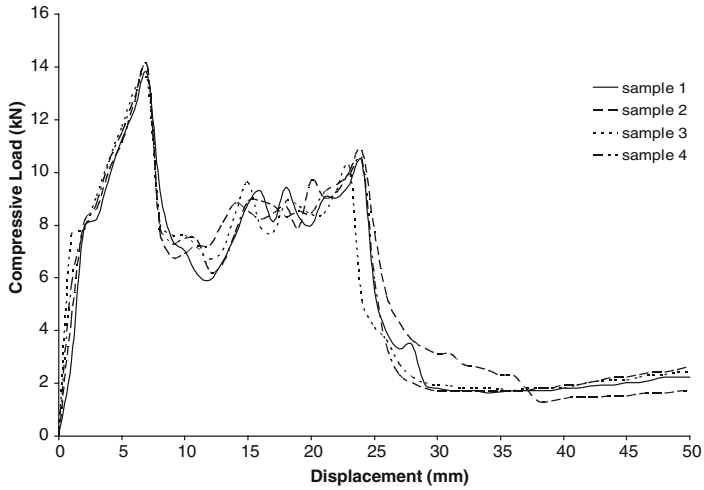

(a) Hexlite 220

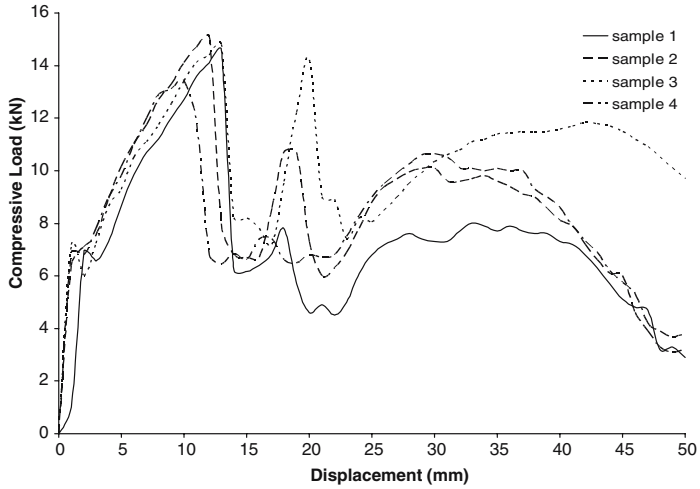

(b) Hexlite 620

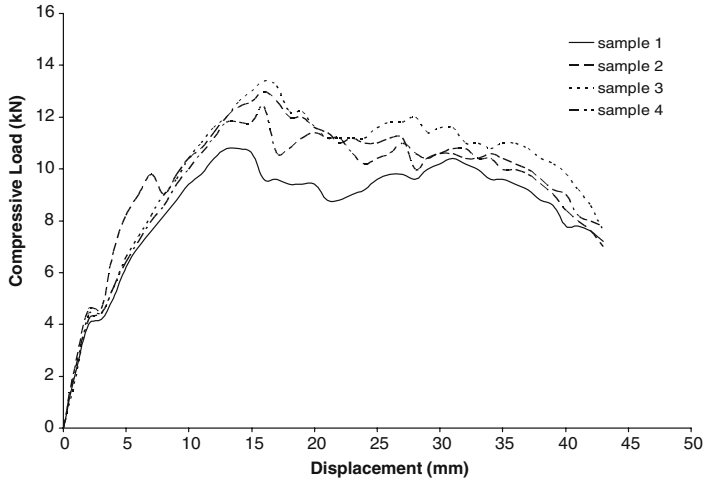

(c) Fibrelam Grade 5

Fig. 2 Load versus displacement data for the truncated cone impactor for four samples of: (**a**) Hexlite H220; (**b**) Hexlite H620; (**c**) Fibrelam Grade 5

For Fibrelam Grade 5, the load versus displacement traces are of a similar shape for the hemispherical and truncated cone impactors but the magnitude of the load was higher for the truncated cone. Related to this, the Fibrelam material exhibited a significant difference in the total energy absorbed for the two different types of impactor head (see Figs. 3b and 11b). This is with energy absorption for the hemispherical impactor of

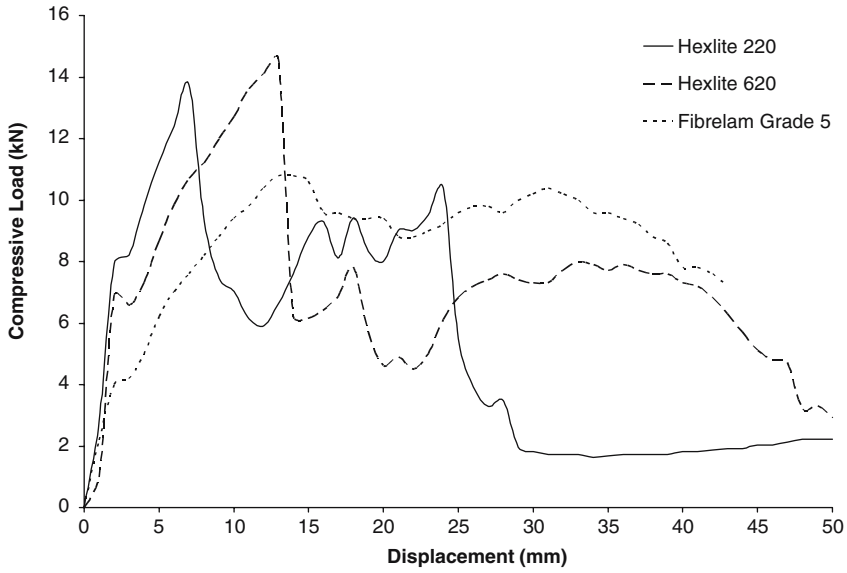

(a) Load versus displacement traces

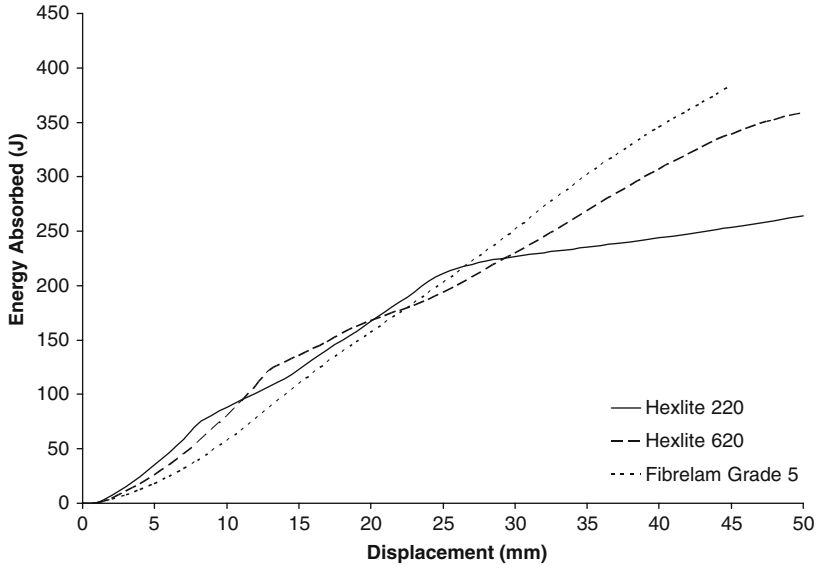

(b) Energy versus displacement traces

Fig. 3 Comparison of H220, H620 and Fibrelam Grade 5 experimental results for truncated cone impactor: (**a**) Load versus displacement traces; (**b**) Energy versus displacement traces

200 J and energy absorption for the truncated cone impactor of nearly 400 J. For both the hemispherical and the truncated cone impactor, there is general deformation of the specimen with little if any loss of bond between skins and honeycomb (see Figs. 6 and 14). Well in evidence are cross-cracks related to the fibre directions in the cross-ply. A point to note is that the initial stiffness and first peak load of the Fibrelam Grade 5 is lower than for H620 and H220 materials for both the hemispherical and truncated cone impactor.

Analysis of impactor geometries

Table 2 compares the results for H220, H620 and Fibrelam Grade 5 materials as determined from load-displacement data for both the truncated cone and hemispherical impactors. This is for when the specimens are clamped in a square frame. For each impactor geometry, the initial slope of the load-displacement trace ($k_{\text{initial}}^{(\text{Expt})}$), the peak load ($F_{\text{peak}}$), the displacement at peak load (x_{peak}) and the total energy absorbed (E_{Total}) are recorded. It is notable that under these loading conditions, the initial specimen stiffness ($k_{\text{initial}}^{(\text{Expt})}$) is higher with the truncated cone impactor than is the case for the hemispherical impactor. The following analysis considers the related contact geometry effects.

For the truncated cone impactor, an early slight depression of the impacted specimen resulted in the impact load quickly being concentrated on the

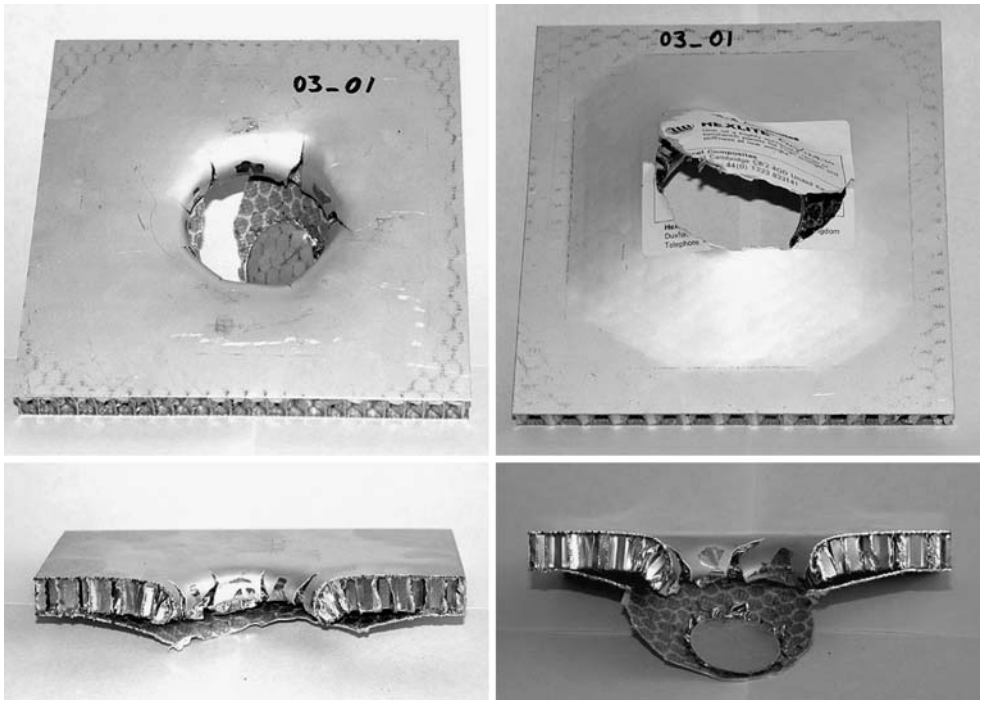

Fig. 4 Damage inflicted on Hexlite H220 for truncated cone impactor (clockwise from top left: top surface, bottom surface and cross sectional views)—Specimen 150 × 150 mm

circumferential edge of the impactor contact face. Therefore, the clamped square specimens were considered as being simply supported at an effective radius of support (a) and the loading due to the truncated cone is assumed spread over a circumferential ring of radius (r_0) from the centre of the specimen. On this basis, the initial deflection of the circumferential loading ring is given approximately by the following relationship [24]:

$$x = f(r_0/a)\left[\frac{Fa^3}{2\pi r_0 D}\right] \tag{1}$$

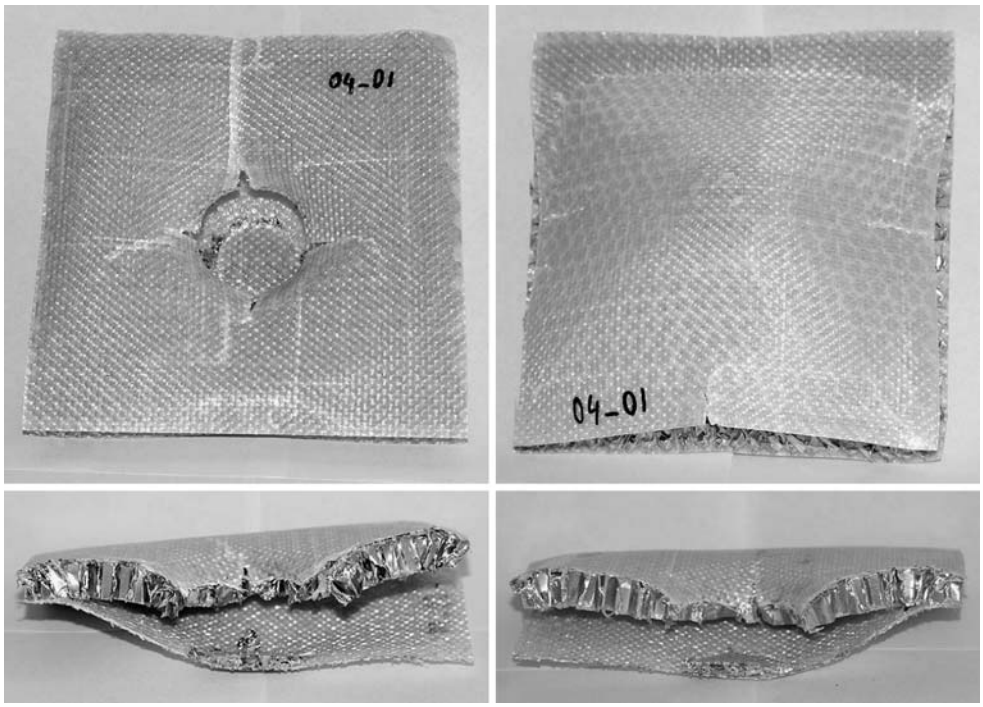

Fig. 5 Damage inflicted on Hexlite 620 for truncated cone impactor (clockwise from top left: top surface, bottom surface and cross sectional views)—Specimen 150 × 150 mm

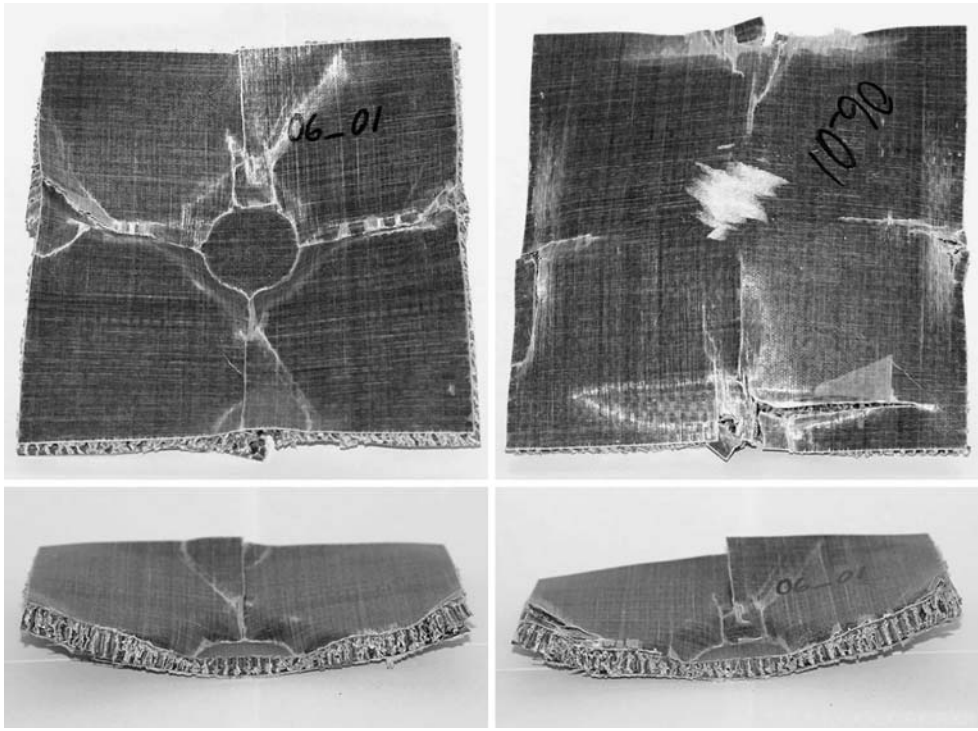

Fig. 6 Damage inflicted on Fibrelam Grade 5 for truncated cone impactor (clockwise from top left: top surface, bottom surface and cross sectional views)—Specimen 150 × 150 mm

where F is the total load on the impactor, $f(r_0/a)$ increases from 0.06 for $r_0/a = 0.2$ up to just less than 0.1 at $r_0/a = 0.5$ and then decreases to 0.06 at $r_0/a = 0.8$ (see Ref. [24]). The plate constant, D, for a material with isotropic in-plane properties would be:

$$D = \left[\frac{E_s t^3}{12\left(1 - \nu_{12}^2\right)}\right] \tag{2}$$

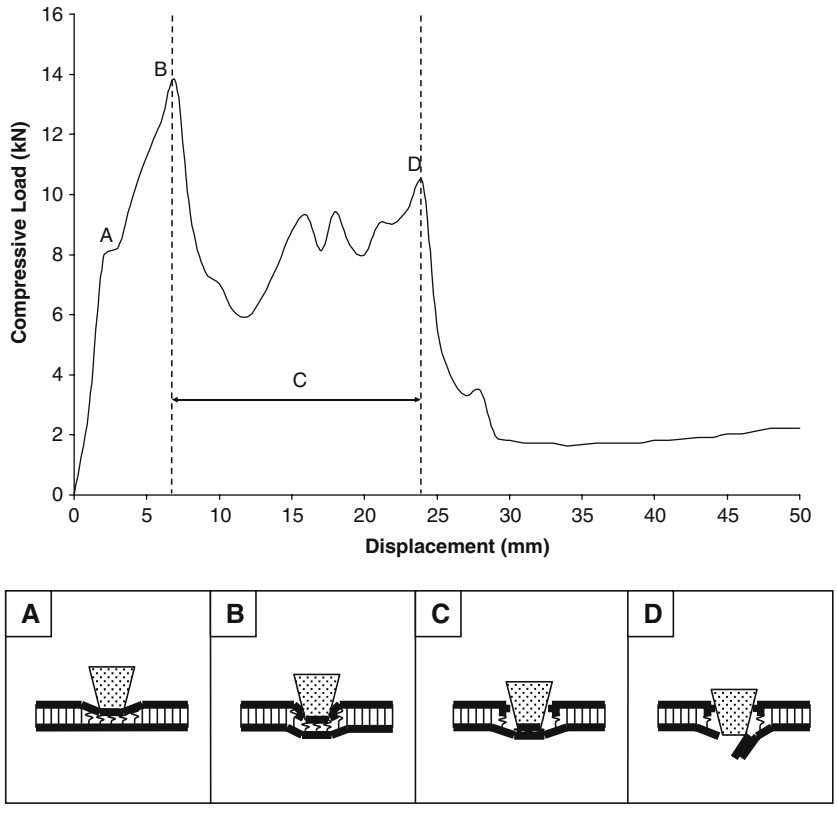

Fig. 7 Load-displacement trace with damage development in Hexlite H220 for truncated cone impactor

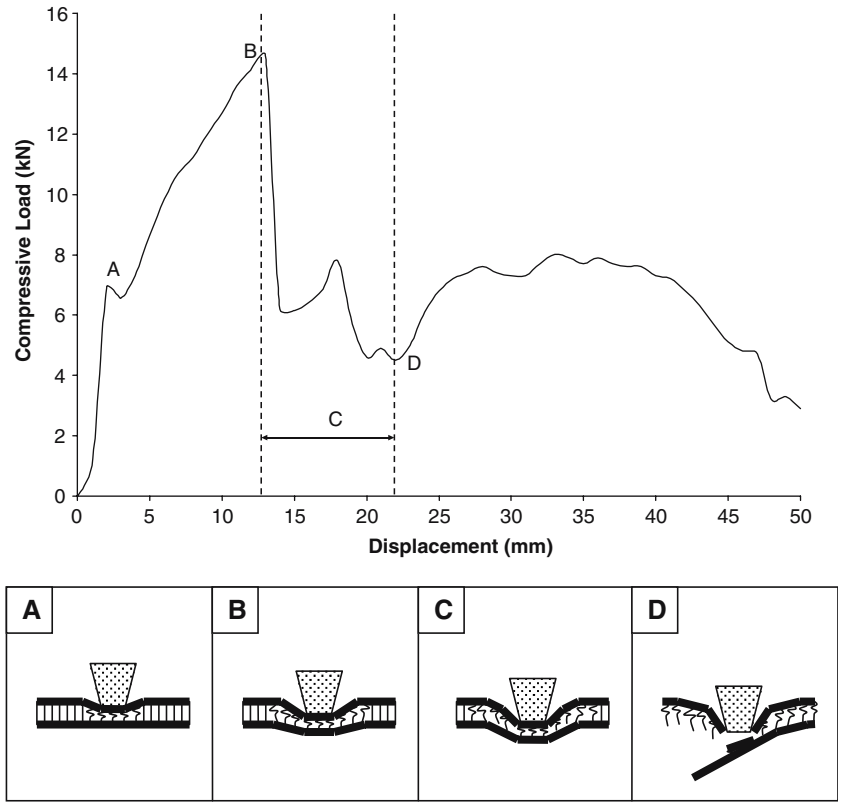

Fig. 8 Load-displacement trace with damage development in Hexlite H620 for truncated cone impactor

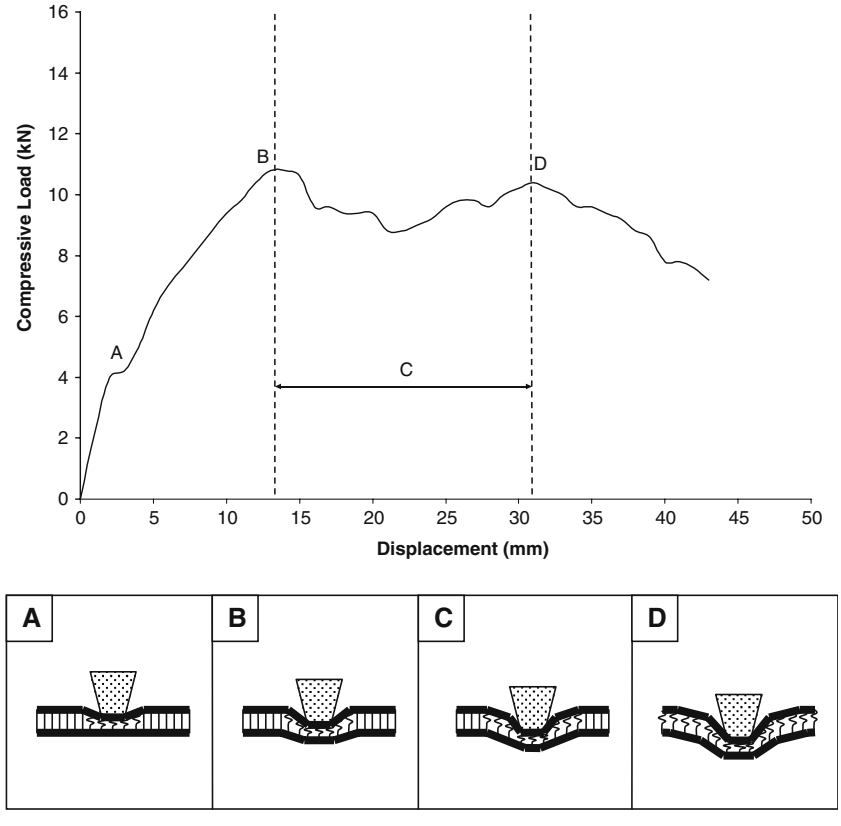

Fig. 9 Load-displacement trace with damage development in Fibrelam Grade 5 for truncated cone impactor

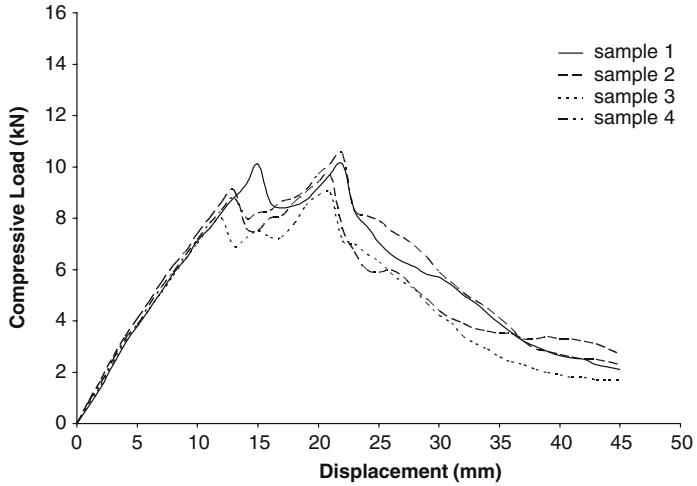

(a) Hexlite 220

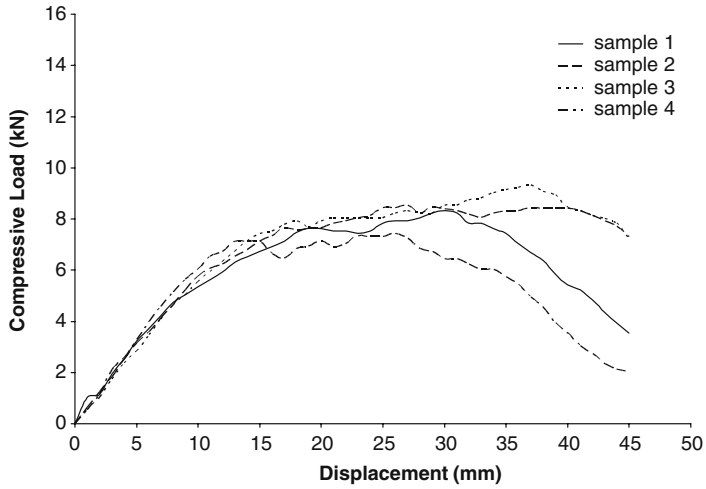

(b) Hexlite 620

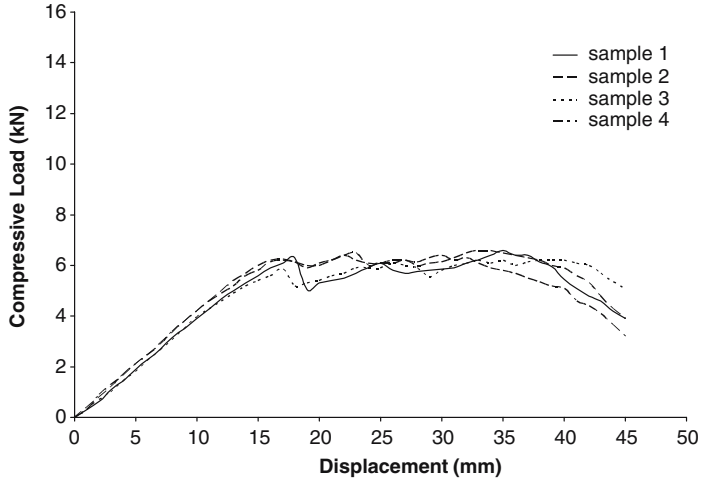

(c) Fibrelam Grade 5

Fig. 10 Load versus displacement data for the hemispherical impactor for four samples of: (**a**) Hexlite H220; (**b**) Hexlite H620; (**c**) Fibrelam Grade 5

where E_s is the in-plane modulus (smeared for the composite skins), v_{12} is the Poisson's ratio and t is the effective thickness of a sheet specimen representing the sandwich panel and having material properties of the skins of the sandwich panel. From Eq. (1), a theoretical relationship for the initial stiffness of the specimen (for small deflections), $k_{\text{initial}}^{(\text{Theory})}$, would be:

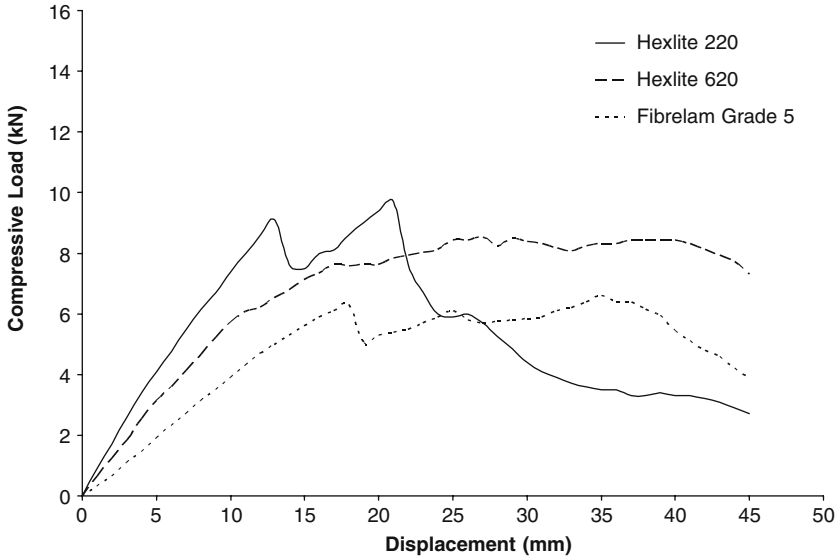

(a) Load versus displacement traces

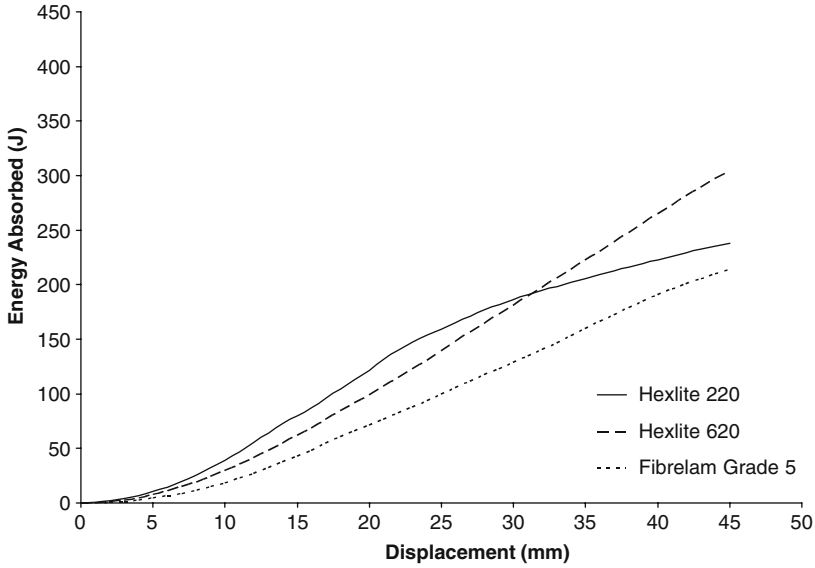

(b) Energy versus displacement traces

Fig. 11 Comparison of H220, H620 and Fibrelam Grade 5 experimental results for hemispherical impactor: (**a**) Load versus displacement traces; (**b**) Energy versus displacement traces

$$k_{\text{initial}}^{(\text{Theory})} = \left[\frac{1}{f(r_0/a)}\right]\left[\frac{2\pi r_0 D}{a^3}\right] \tag{3}$$

with the plate constant, D, for each material defined by Eq. (2).

Likewise, for the hemispherical impactor, the clamped square specimens are considered as being simply supported at an effective radius, a, from the centre and the initial contact loading is assumed to be spread over a very small circular area at the centre of the specimen. For this case, the initial load point deflection, x, for a sheet specimen is given approximately by the following relationship [24]:

$$x = \left[\frac{Fa^2}{16\pi D}\right]\left[\frac{3+v}{1+v}\right] \tag{4}$$

where F is the central load. From Eq. (4), a theoretical relationship for the initial stiffness of the specimen ($k_{\text{initial}}^{(\text{Theory})}$) for small deflections would be:

$$k_{\text{initial}}^{(\text{Theory})} = \left[\frac{16\pi D}{a^2}\right]\left[\frac{1+v}{3+v}\right] \tag{5}$$

with the plate constant, D, defined by Eq. (2). The effective radius of support (a) was identified that provided a good link between the theoretical and

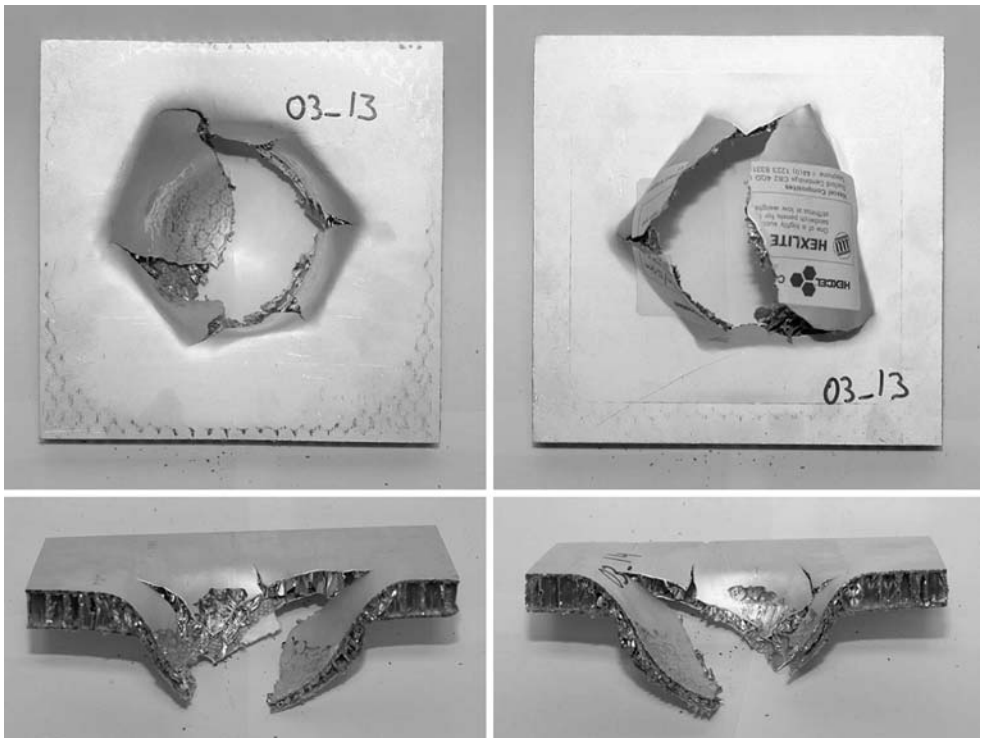

Fig. 12 Damage inflicted on Hexlite H220 for hemispherical impactor (clockwise from top left: top surface, bottom surface and cross sectional views)—Specimen 150 × 150 mm

experimental data. Table 2 compares the theoretical values for the initial specimen stiffness ($k_{\text{initial}}^{(\text{Theory})}$) with the experimental values of stiffness ($k_{\text{initial}}^{(\text{Expt})}$) as determined from the initial slope of the load-displacement traces for the three sandwich materials and the two different loading geometries. For the sandwich panels with composite skin, the modulus was the in plane smeared tensile modulus of the composite skin. With the above reasoning, then, for both the truncated cone and hemispherical loading geometry, the same effective radius of support (a) could be used to make a useful comparison between predicted and measured

Fig. 13 Damage inflicted on Hexlite 620 for hemispherical impactor (clockwise from top left: top surface, bottom surface and cross sectional views)—Specimen 150 × 150 mm

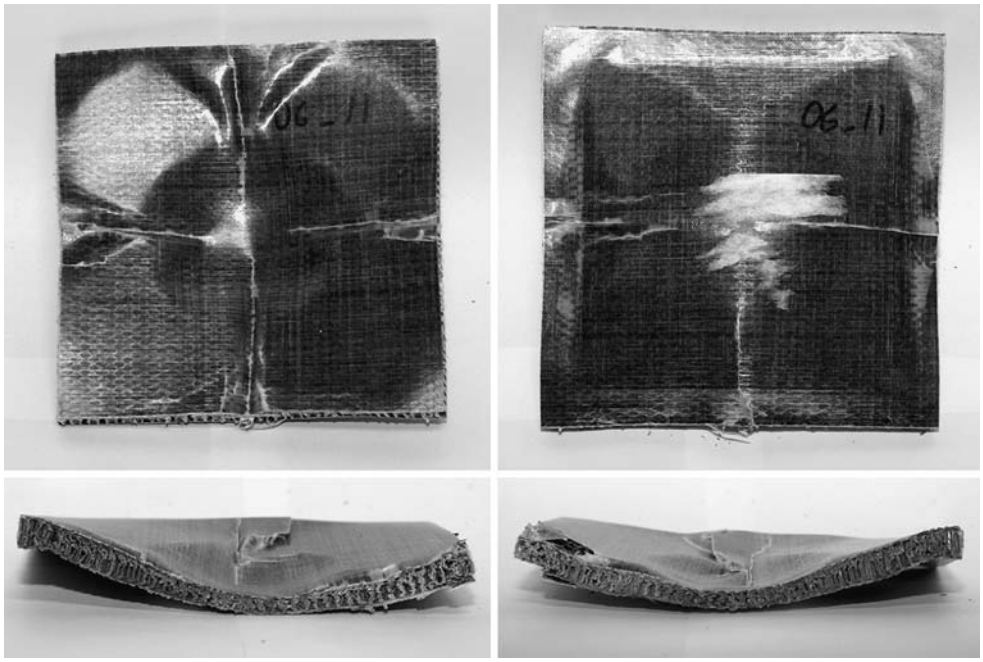

Fig. 14 Damage inflicted on Fibrelam Grade 5 for hemispherical impactor (clockwise from top left: top surface, bottom surface and cross sectional views)—Specimen 150 × 150 mm

stiffness. To be noted is that the theoretically and experimentally determined initial specimen stiffnesses for the hemispherical impactor are approximately 20% of the initial specimen stiffness for the truncated cone impactor. It can be seen that initial contact geometry is an important factor in determining loading response and subsequent damage development. The early contact damage and the distribution of the stresses on the sandwich panels much relates to this initial specimen stiffness.

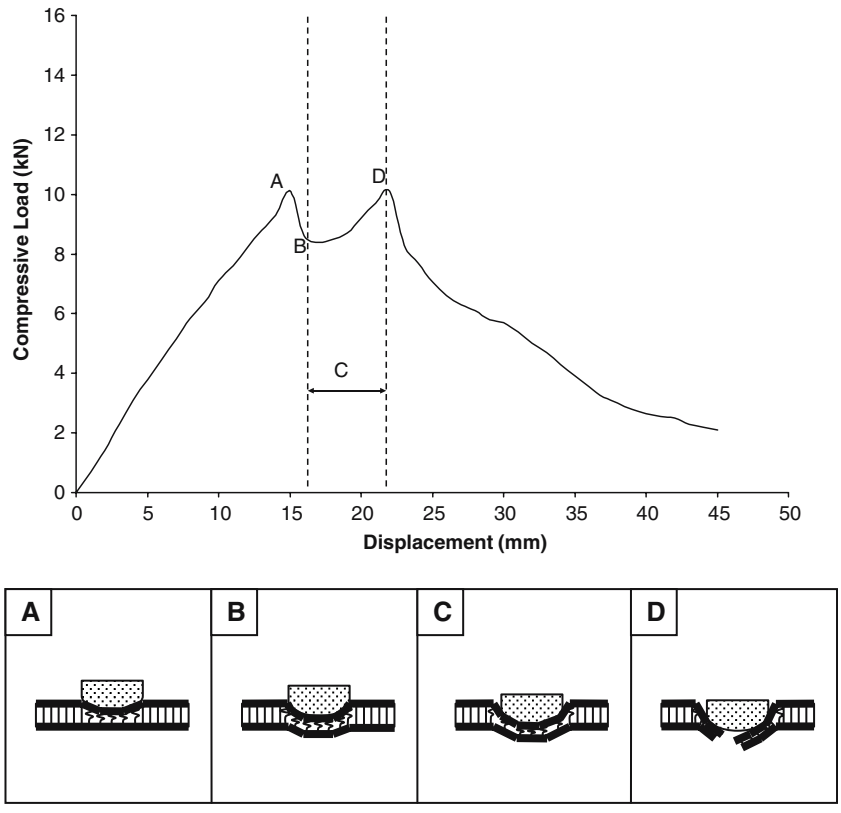

Fig. 15 Load-displacement trace with damage development in Hexlite H220 for hemispherical impactor

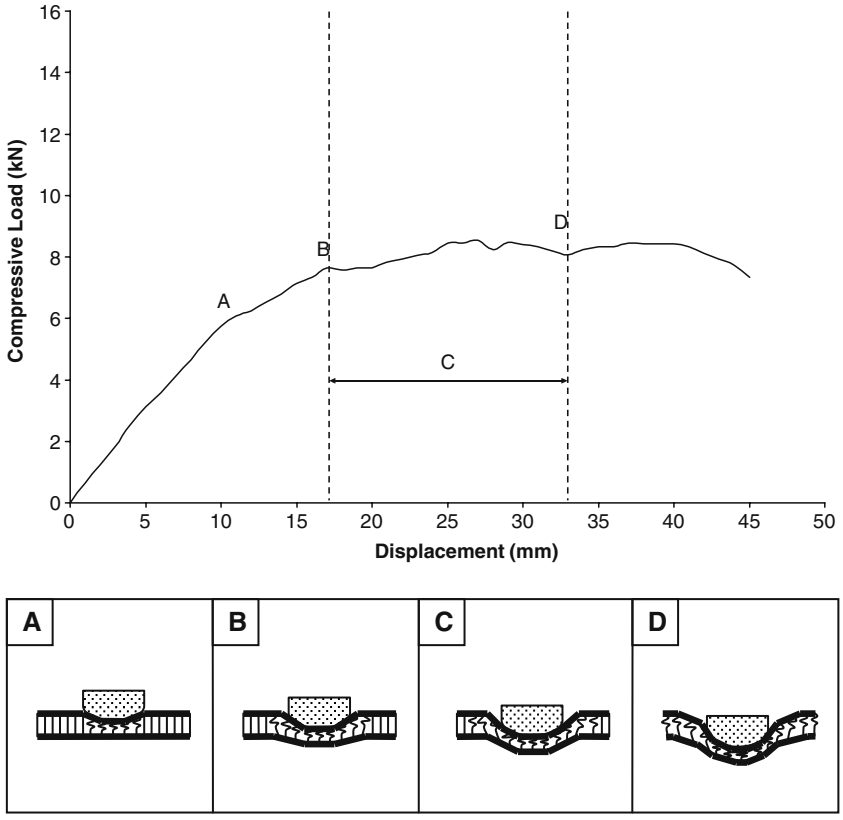

Fig. 16 Load-displacement trace with damage development in Hexlite H620 for hemispherical impactor

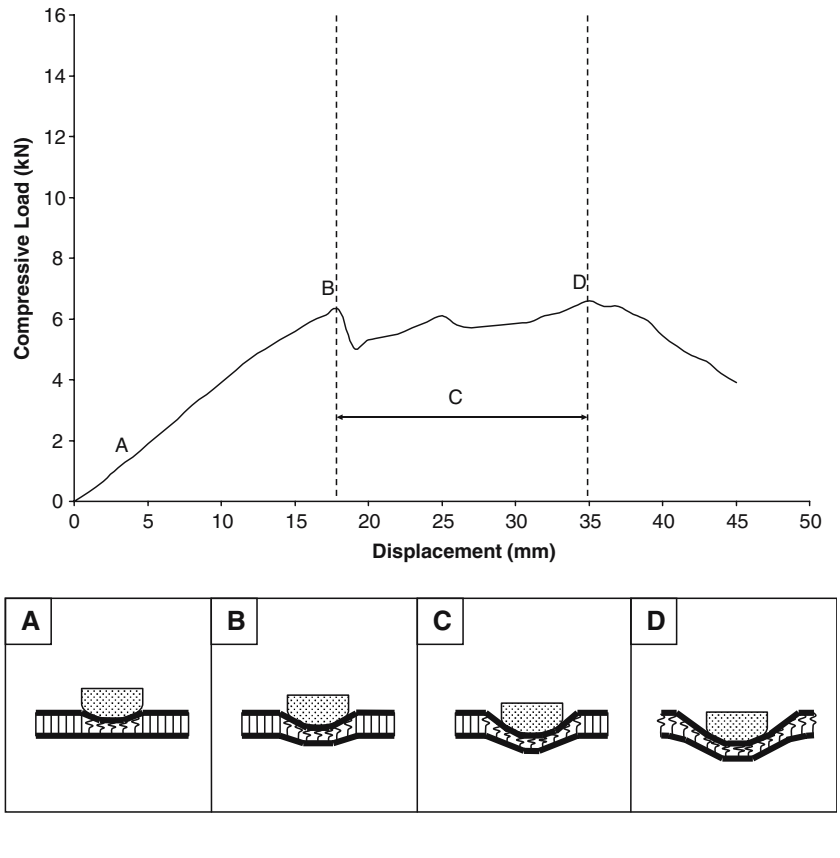

Fig. 17 Load-displacement trace with damage development in Fibrelam Grade 5 for hemispherical impactor

Table 2 Stiffness, peak load and energy absorbed for different impact geometries

	Hexlite H220	Hexlite H620	Fibrelam Grade 5
(a) Truncated cone impactor results			
Initial stiffness—$k_{\text{initial}}^{(\text{Expt})}$ (MN/m)	4	3	2
First peak load—F_{peak} (kN)	14	15	11
Displacement at first peak load—x_{peak} (mm)	7	13	14
Total energy absorbed—E_{Total} (J)	260	350	400
Smeared skin modulus—E_{s} (GPa)	70	30	34
Poisson's ratio of skin material—v_{12}	0.3	0.3	0.3
Effective plate constant—D (N m)	24	9.3	6.8
Effective plate support radius—a (m)	0.021	0.021	0.021
Truncated cone impactor face radius—r_0 (m)	0.0165	0.0165	0.0165
Effective plate thickness—t (m)	0.0015	0.0015	0.0013
Theoretical initial stiffness—$k_{\text{initial}}^{(\text{Theory})}$ (MN/m)	4.3	1.7	1.2
Based on a ring loaded plate—see Eq. 3			
Peak stiffness—$k_{\text{peak}}^{(\text{Expt})}$ (MN/m) (=$F_{\text{peak}}/x_{\text{peak}}$)	2	1.2	0.78
$k_{\text{peak}}^{(\text{Expt})}/k_{\text{initial}}^{(\text{Expt})}$	0.5	0.4	0.39
(b) Hemispherical impactor results			
Initial stiffness—$k_{\text{initial}}^{(\text{Expt})}$ (MN/m)	0.7	0.48	0.4
First peak load—F_{peak} (kN)	9	8.5	6
Displacement at first peak load—x_{peak} (mm)	13	25	18
Total energy absorbed—E_{Total} (J)	230	300	200
Smeared skin modulus—E_{s} (GPa)	70	30	34
Poisson's ratio of skin material—v_{12}	0.3	0.3	0.3
Effective plate constant—D (N m)	24	9.3	6.8
Effective plate support radius—a (m)	0.021	0.021	0.021
Effective plate thickness—t (m)	0.0015	0.0015	0.0013
Theoretical initial stiffness—$k_{\text{initial}}^{(\text{Theory})}$ (MN/m)	1.0	0.42	0.31
Based on a centrally loaded plate—see Eq. 5			
Peak stiffness—$k_{\text{peak}}^{(\text{Expt})}$ (MN/m) (=$F_{\text{peak}}/x_{\text{peak}}$)	0.69	0.34	0.33
$k_{\text{peak}}^{(\text{Expt})}/k_{\text{initial}}^{(\text{Expt})}$	0.99	0.71	0.83

It is also interesting to note, from Table 2, that if specimen stiffness associated with the peak load of the load-displacement trace is calculated from:

$$k_{\text{peak}}^{(\text{Expt})} = \left[\frac{F_{\text{peak}}}{x_{\text{peak}}}\right] \tag{6}$$

then, the ratio $k_{\text{peak}}^{(\text{Expt})}/k_{\text{initial}}^{(\text{Expt})}$ reduces from 50% for H220 to 39% for Fibrelam Grade 5 for the truncated cone impactor and $k_{\text{peak}}^{(\text{Expt})}/k_{\text{initial}}^{(\text{Expt})}$ reduces from 99% for H220 to 71% for H620 for the hemispherical impactor. Related to this, for the hemisperical impactor very little front surface contact deformation or rear surface damage is observed up to the peak load condition. However, for the truncated cone impactor, there is evidence of the impactor bedding more into the sandwich material, deforming the top skin and crushing core material that produces a characteristic small dip in the initial part of force-displacement trace.

Discussion

The method of driving impactors with different head geometry at constant velocity into honeycomb sandwich material until the impact head penetrates the material to the required degree has many assessment advantages. For example, in this constant displacement rate method, the variation in monitored force only relates to the resistance of the specimen as it reaches and goes through its different failure modes. This is helpful in distinguishing between the resistance offered by the top skin as it deforms and fails, the crushing of the honeycomb core and then the failure of the rear skin. It is to be noted that in the case of the truncated cone impactor, following the early depression of the impacted specimen, the impact force is concentrated on the circumferential edge of the impactor contact face. This resulted in a failure process starting from the edge of the circular hole in the front skin. For some materials, this can be part of the early bedding in of the impactor into the sandwich core material. This relates to the early small dip in the first rising part of the load-displacement traces for the truncated cone impactor.

A difference between H220 and H620 sandwich structures is that the skins for H220 are aluminium and for H620 they are woven glass fibre impregnated with epoxy resin. In both cases, the core is of the same aluminium honeycomb material and construction. Notable is that for both the truncated cone and the

hemispherical impactor, there is little variability in the results of the four H220 specimens assessed. In the case of H620, there was more variability in the load versus displacement traces for the four specimens particularly for the truncated cone impactor. A reason for this is that the edge of the truncated cone impactor in generating a circular fracture of the aluminium front skin of H220 also gathered and rolled inwards a ring of the skin material around the circumference of the hole. Also, mostly due to this circular perforation of the front skin, most of the damage to the H220 core, at least in the early damage phase, was very confined. However, in the case of H620, the truncated cone impactor started a more complex fracture pattern as it started to hole the woven glass fibre/epoxy skin. This is with the top skin suffering radial cracks and there was more general delamination of the rear composite skin that took up a domed shape. In terms of impact energy absorption, H220 absorbed similar energy for the truncated cone or hemispherical impactor although the failure modes for the two impactor types differed. The H620 specimens had more extensive damage and particularly notable was the increase in impact energy absorption for displacements beyond 25 mm. This was the case for both the truncated cone and hemispherical impactor. For displacements beyond 25 mm in H220 specimens for the truncated cone impactor, there was a dramatic reduction in impact force with displacement. This is because the damage was more centralised. However, for some applications, H220 is usefully a stiffer sandwich structure.

With the hemispherical impactor, for both H220 and H620 materials, there is less distinction between the initial elastic response and the onset of the damaging processes. This is mostly due to the increasing contact area that spreads the load. This illustrates one needed design consideration for the use of sandwich honeycomb materials. The open door type of rear skin failure of sandwich materials often occurs if the impactor holes the front skin or for other reasons the compacting of the core is closely confined through to the rear skin. This was very much in evidence with H220 for the truncated cone impactor whereas this was less in evidence for the hemispherical impactor because of the increasing contact area widely spreading the impact loading.

The failure of the Fibrelam Grade 5 material with its unidirectional cross-plied fibreglass skins and aramid core demonstrated well the importance of the type of skins on the damage inflicted on the honeycomb core material. For Fibrelam Grade 5, the honeycomb aramid core has the same core density as for the aluminium core used in H220 and H620. In the case of the Fibrelam material, the truncated cone impactor initially formed a circular indentation in the skin material with partial radial cracks dividing the skin material into four approximately equal parts. The result was the whole of the Fibrelam specimen became bowed and there was no central full penetration through the thickness of the specimen. To be noted is that as the honeycomb became compacted under the impactor so the rear skin developed cross-cracks but without an open rear door fracture. In the case of the hemispherical impactor, absent is the circular indentation at the centre of the top skin but again the partial radial cracks divide the top skin into four separated square areas. This resulted in a wider compaction of the honeycomb core and cross cracking of the rear skin. Interestingly, there was a very big difference in the energy absorbed from the truncated cone and the hemispherical impactors. This is with the energy absorbed from the truncated cone impactor being about twice that of the hemispherical impactor. This was mostly because of the larger initial contact area of the truncated cone impactor causing wider compacting of the core than in the case of the hemispherical impactor.

Conclusions

In this study, the key requirements were to relate the stiffness of sandwich panels to their impact failure processes for specific impact conditions in terms of the size of the contact zone and specimen support arrangements. This was to provide for evaluating a wide range of sandwich materials of the type researched in this study for different impact conditions. Also, needed was to be able to determine the contribution to stiffness and damage tolerance of the skins, core material and their bonding. The data obtained was particularly informative for the honeycomb materials to be used for racing cars when the crash impacts can be extremely severe. However, with faster and denser traffic conditions for all types of transport and the increased use of sandwich honeycomb and other lightweight materials, it is becoming increasingly important to provide similar data for designing impact safety barriers for drivers and occupants of cars, railway coaches and other vehicles.

Acknowledgements The authors thank Hexcel Composites for providing samples for the experiments.

References

1. Federation International du Sport Automobile, 2000/01—excerpts from formula one world championship technical regulations 2001, published: 02/11/2000

2. Savage G (1992) Met Mater 8:147
3. Gibson LJ, Ashby MF (1988) Cellular solids: structure and properties. Pergamon Press, Oxford, p 241
4. Abrate S (1998) Impact on composite structures. Cambridge University Press, Cambridge, p 1
5. Davies GAO, Zhang X (1995) Int J Impact Eng 16:149
6. Olsson R (2001) Compos: Part A 32: 1207
7. Robinson P, Davies GAO (1992) Int J Impact Eng 12:189
8. Gong SW, Lam KY (1999) Compos: Part B 30:473
9. Bland PW (2000) Impact response and performance of carbon–fibre reinforced polymers. PhD Thesis, Imperial College of Science, Technology and Medicine, University of London
10. Brown SA (1999) Low velocity impact resistance of reinforced polymeric materials. PhD Thesis, Imperial College of Science, Technology and Medicine, University of London
11. Harrigan JJ, Reid SR, Peng C (1999) Int J Impact Eng 22:955
12. Langdon GS, Cantwell WJ, Nurick GN (2005) Compost Sci Technol 65:861
13. Grant PV, Cantwell WJ, McKenzie H, Corkhill P (1998) Int J Impact Eng 21:737
14. Cantwell WJ (1996) J Comp Mat 30:1266
15. Herup EJ, Palazotto AN (1997) Compos Sci Technol 57:1581
16. Abrate S (1997) Appl Mech Rev 50:69
17. Mines RAW, Worrall CM, Gibson AG (1998) Int J Impact Eng 21:855
18. Olsson R (2002) J Sandwich Struct Mat 4:3
19. Anderson T, Madenci E (2000) Compos Struct 50:239
20. Akil Hazizan Md, Cantwell WJ (2003) Compos: Part B 34:679
21. Roach AM, Evans KE, Jones N (1998) Compos Struct 42:135
22. Shyr T-W, Pan Y-H (2004) Compos Struct 64:189
23. Maruszewska W (2005) Failure processes in composite sandwich structures for automotive and similar applications. PhD Thesis, Imperial College London, University of London
24. Young WC (1989) Roark's formulas for stress and strain. McGraw-Hill: New York, p 398